EVS35 Symposium
Oslo, Norway, June 11-15, 2022

A Model Predictive Control-Based State of Power Estimation Algorithm Using Adaptive Weighting

Aloisio Kawakita de Souza[1,2], Gregory L. Plett[1,3], M. Scott Trimboli[1,4]
[1]*Department of Electrical and Computer Engineering, University of Colorado Colorado Springs, Colorado Springs, CO 80918, United States*
[2]akawakit@uccs.edu, [3]gplett@uccs.edu, [4]mtrimbol@uccs.edu

Summary

Dynamic power management (DPM) is a critical element for ensuring safe and efficient energy utilization for electric vehicles (EVs). Key to effective DPM is the ability to supply the battery management system (BMS) with timely and accurate estimates of battery state of power (SOP). This paper presents a robust algorithm for SOP computation using a model predictive control (MPC) framework and a coupled electro-thermal equivalent circuit model (ECM). The method incorporates a novel adaptive strategy for adjusting MPC parameters in order to improve accuracy and increase algorithm robustness.

1 Abstract

State of power (SOP) estimation is crucial for high performance battery applications such as those powering battery electric vehicles (BEVs). Near-real-time estimates of SOP allow a vehicle controller to apportion available power in a safe and efficient manner. Since no sensors exist to determine available power directly, it must be estimated from measurements of current, voltage, and temperature. A variety of methods for SOP estimation appear in the literature, ranging from offline computations, [1,2] to online model-based techniques, e.g., [3–12].

A predictive estimate of power is preferred to an instantaneous estimate to allow for load planning over a specified time horizon. In line with this, an approach has been inspired by model predictive control (MPC) [12] whereby a prediction of future cell states is used to compute step-wise optimal inputs to satisfy a performance objective while observing constraints on designated system variables. Implementation of this method, however, requires careful choice of MPC tuning parameters to ensure accurate and robust performance. Since the algorithm is carried out in real-time, execution of MPC at each sampling instant can encounter a widely varying set of operating conditions which could adversely affect SOP estimation accuracy. Our contribution in this paper is the introduction of an adaptive input weighting scheme to improve both the accuracy and robustness of the MPC-based SOP calculations. We call the proposed method s*elf-adaptive MPC* (SAMPC).

This paper builds on the work in [12] which formulated a low-cost, MPC-based method to compute an accurate estimate of available charge and discharge power over a finite horizon. Specifically, the method executes constrained, linear MPC at each sample point to predict an optimal future power profile and then numerically integrates power to compute total energy. It then averages the result to estimate maximum sustainable power. Importantly, in this framework, MPC is not used to control the battery, but rather to inform the BMS.

2 Self-adaptive model predictive control formulation

In [12] we introduced a state of power estimation approach using a standard linear MPC formulation that solves a tracking problem in terms of state of charge in order to compute maximum charge and discharge power. It was shown there that a quadratic objective function minimized by a light-weight quadratic programming (QP) solver based on the Hildreth algorithm [13] can be implemented at low computational cost. Although effective, the technique exhibited sometimes wide variations in the point-wise MPC calculation of estimated power. This was later discovered to be caused by the choice of a single set of MPC tuning parameters for the entirety of the vehicle's operating range.
In order to address this shortcoming, we introduce a modification to our previous SOP estimation algorithm whereby we assign the control weight tuning parameter dynamically at each time step based on a simple norm-based measure of a certain matrix size.
In this section we describe the details of the self-adaptive MPC-based framework. We begin with a brief overview of the standard linear MPC algorithm followed by a derivation of the adaptive input weighting technique and its application to our SOP formulation.

2.1 MPC Optimization Fundamentals

The proposed SOP algorithm uses the prediction/optimization functions of the standard linear MPC algorithm described for the lithium-ion fast-charge problem in [14]. There, an objective function was specially designed to bring the battery state-of-charge to a target value in minimum time. We shall utilize the same set-up here and summarize its main features below.

2.1.1 Output prediction

The heart of the MPC algorithm is the prediction of future outputs. For a linear state-space model, the output prediction is a linear function of an augmented state vector $\boldsymbol{\chi}_k$ and the vector of future input increments $\underrightarrow{\Delta \boldsymbol{u}}_{k+1}$

$$\underrightarrow{\boldsymbol{y}}_{k+1} = \Phi \tilde{A} \boldsymbol{\chi}_k + G \underrightarrow{\Delta \boldsymbol{u}}_{k+1}, \tag{1}$$

where $\underrightarrow{\boldsymbol{y}}_{k+1} \in \mathbb{R}^{2 \cdot N_\mathrm{p}}$ is a vector containing all future output predictions and $\underrightarrow{\Delta \boldsymbol{u}}_{k+1} \in \mathbb{R}^{2 \cdot N_\mathrm{c}}$ is a vector containing all future control input increments. Integers N_p and N_c denote the sample-length of the prediction and control horizons, respectively. Matrices $\Phi \in \mathbb{R}^{2 \cdot N_\mathrm{p} \times (N_x+2)}$ and $G \in \mathbb{R}^{2 \cdot N_\mathrm{p} \times 2 \cdot N_\mathrm{c}}$ are built from augmented state space matrices $\tilde{A}$, $\tilde{B}$, and $\tilde{C}$ when propagating both states and output through the range of the prediction horizon[1]. It is important to note that the battery system is non-strictly causal due to its ohmic resistance; therefore, this formulation assumes at present time sample k the 'current' control input $\boldsymbol{u}_k$ has been computed previously (at time sample $k-1$) and then uses this information together with present state information contained in $\boldsymbol{\chi}_k$ to compute the future control increment $\Delta \boldsymbol{u}_{k+1}$ according to the receding horizon principle.

2.1.2 Quadratic optimization problem

The MPC objective function is defined as:

$$J_k = \left\| \underrightarrow{\boldsymbol{r}}_{k+1} - \underrightarrow{\boldsymbol{y}}_{k+1} \right\|_S^2 + \left\| \underrightarrow{\Delta \boldsymbol{u}}_{k+1} \right\|_{\bar{R}}^2, \tag{2}$$

where $\underrightarrow{\boldsymbol{r}}_{k+1} = y_\mathrm{ref} \cdot \mathbf{e}$. Here, y_ref is the target output reference, $\mathbf{e}$ is a column vector of ones, and S and $\bar{R}$ are output and input weighting matrices, respectively. For simplicity, we set $S = I_{N_\mathrm{p}}$ and $\bar{R} = \rho_k I_{N_\mathrm{c}}$, where ρ_k is a tuning parameter that penalizes the size of the input increment. The identity matrices are dimensioned by the length of the respective horizons. Substituting (1) into (2), expanding terms and considering only those terms containing $\underrightarrow{\Delta \boldsymbol{u}}_{k+1}$ gives the following quadratic form:

$$J_k = \underrightarrow{\Delta \boldsymbol{u}}_{k+1}^\mathsf{T} H \underrightarrow{\Delta \boldsymbol{u}}_{k+1} + \underrightarrow{\Delta \boldsymbol{u}}_{k+1}^\mathsf{T} \boldsymbol{g}, \tag{3}$$

where

$$H = G^\mathsf{T} G + \rho_k I_{N_\mathrm{c}}, \; \boldsymbol{g} = -2 G^\mathsf{T} (\underrightarrow{\boldsymbol{r}}_{k+1} - \Phi \tilde{A} \boldsymbol{\chi}_k) \tag{4}$$

[1] Strictly speaking, matrices $\tilde{A}$, $\tilde{B}$, and $\tilde{C}$ are time-varying; however for clarity in this development we omit explicit time-dependence for these terms.

At each sampling instant, the MPC algorithm solves the following constrained optimization problem:

$$\min_{\underrightarrow{\Delta \boldsymbol{u}}_{k+1}} \quad J_k, \quad s.t.\ M\underrightarrow{\Delta \boldsymbol{u}}_{k+1} \leq \boldsymbol{\gamma} \tag{5}$$

where matrix M and vector $\boldsymbol{\gamma}$ are defined according to the constraint equations. Although the solution used in the SOP algorithm is ultimately generated by solving the constrained optimization problem, the self-adaptive scheme uses the unconstrained problem as its basis; its solution is found by solving (5) to obtain,

$$\underrightarrow{\Delta \boldsymbol{u}}^*_{k+1} = -\frac{1}{2}H^{-1}\boldsymbol{g} \tag{6}$$

where $\underrightarrow{\Delta \boldsymbol{u}}^*_{k+1}$ is the vector of optimal future input increments for the unconstrained case.[2]

2.1.3 State-space MPC with feedthrough

It is important that models of lithium-ion battery dynamics include a non-zero feedthrough term to account correctly for ohmic resistance in the cell. This is a modification to the standard MPC algorithm and can be accomplished by re-defining the augmented state vector $\boldsymbol{\chi}_k$ to contain both the system states $\boldsymbol{x}$ and the system input $\boldsymbol{u}$. Details can be found in [15].

2.2 Adaptive input weighting

The essential idea of adaptive input weighting is to select a value for ρ_k that will result in an optimal unconstrained input value that is in some sense "close" to the size of the input constraint limit. It has been found in practice that by doing so, the iterative Hildreth quadratic programming scheme converges more quickly to the correct constrained solution, thus eliminating the variation in SOP estimates seen previously.

Utilizing the vector-matrix 2-norm, we apply the triangle inequality to express an upper bound on (6) as

$$\begin{aligned}\left\|\underrightarrow{\Delta \boldsymbol{u}}^*_{k+1}\right\| &\leq \frac{1}{2}\left\|H^{-1}\boldsymbol{g}\right\| \\ &\leq \frac{1}{2}\left\|H^{-1}\right\|\|\boldsymbol{g}\| \\ &\leq \frac{1}{2}\left\|\left(G^{\mathsf{T}}G+\rho_k I\right)^{-1}\right\|\|\boldsymbol{g}\|. \end{aligned} \tag{7}$$

In order to obtain an absolute magnitude-based algorithm, we re-write (7) by equating the right-hand side upper bound directly to the constraint value, yielding

$$\left\|\left(G^{\mathsf{T}}G+\rho_k I\right)^{-1}\right\| = \frac{2\overline{\Delta u}\sqrt{N_{\mathrm{c}}}}{\|\boldsymbol{g}\|} \tag{8}$$

where the overbar denotes an upper bound value. Note that the norm of the inverse of a matrix $\boldsymbol{P}$ may be expressed as

$$\left\|P^{-1}\right\| = \frac{1}{\underline{\sigma}\left(P\right)} \tag{9}$$

where $\underline{\sigma}\left(\cdot\right)$ denotes the minimum singular value. In the case where P is positive definite symmetric, $\underline{\sigma}\left(P\right) = \sqrt{\underline{\lambda}\left(P\right)}$ where $\lambda\left(\cdot\right)$ represents the eigenvalue spectrum of P. Therefore, substituting the form of the norm inverse from (9) into (8) yields

$$\frac{1}{\underline{\sigma}\left(G^{\mathsf{T}}G+\rho_k I_{N_{\mathrm{c}}}\right)} = \frac{2\overline{\Delta u}\sqrt{N_{\mathrm{c}}}}{\|\boldsymbol{g}\|} \tag{10}$$

and rearranging,

$$\underline{\sigma}\left(G^{\mathsf{T}}G+\rho_k I_{N_{\mathrm{c}}}\right) = \frac{\|\boldsymbol{g}\|}{2\overline{\Delta u}\sqrt{N_{\mathrm{c}}}}. \tag{11}$$

Solving for ρ_k gives the result,

$$\rho_k = \frac{\|\boldsymbol{g}\|}{2\overline{\Delta u}\sqrt{N_{\mathrm{c}}}} - \underline{\sigma}\left(G^{\mathsf{T}}G\right). \tag{12}$$

[2] Note that in the standard MPC algorithm, the unconstrained solution is already computed to determine if the more expensive quadratic program needs to execute.

Charge	Discharge
$z_k \leq z_{\max}$	$z_k \geq z_{\min}$
$v_k \leq v_{\max}$	$v_k \geq v_{\min}$
$i_{\min} \leq i_k \leq 0$	$0 \leq i_k \leq i_{\max}$
$T_{c,k} \leq T_{\max}$	$T_{c,k} \leq T_{\max}$

Table 1: SOP constraints.

3 An MPC-inspired State of Power estimation method

The MPC framework developed in Section 2 is employed in an iterative, step-wise algorithm to compute a fast-charge and fast-discharge optimal profile that is used to estimate the battery SOP. This involves first finding the input current profile required to bring a battery cell from an initial SOC to a final SOC in the shortest possible time. Recognizing this is a min-time optimal control problem (and notoriously difficult to solve), we instead fashion a *pseudo* min-time problem (PMTP) [14] designed to give essentially the same result. Moreover, it has been shown in [16] that the PMTP can also deliver a solution to the maximum available power problem.

If we define the state of charge z as the controlled variable and the input current increment Δi as the system input (as defined in (2)), we can re-write the PMTP objective function as:

$$J_k = \left\| \underrightarrow{\boldsymbol{r}}_{k+1} - \underrightarrow{\boldsymbol{z}}_{k+1} \right\|_S^2 + \left\| \underrightarrow{\Delta \boldsymbol{i}}_{k+1} \right\|_{\bar{R}}^2, \tag{13}$$

where $\underrightarrow{\boldsymbol{z}}_{k+1} \in \mathbb{R}^{N_\mathrm{p}}$ is a vector of future SOC predictions, $\underrightarrow{\boldsymbol{r}}_{k+1} = z_{\text{final}} \cdot \boldsymbol{e}$, and $\underrightarrow{\Delta \boldsymbol{i}}_{k+1} \in \mathbb{R}^{N_\mathrm{c}}$ is a vector of predicted input currents. It turns out, the optimization problem

$$\min_{\underrightarrow{\Delta \boldsymbol{i}}_{k+1}} \quad J_k, \quad \text{s.t. } M \underrightarrow{\Delta \boldsymbol{i}}_{k+1} \leq \boldsymbol{\gamma} \tag{14}$$

is made more computationally efficient by solving instead the corresponding dual quadratic programming (QP) problem [14]. The QP solver implemented in this work is an iterative Gauss-Seidel variant proposed by Hildreth [13]. The method utilizes a primal-dual approach [17] to solve a linear system of equations using an element-by-element reduction which avoids matrix inversion. The algorithm has been shown to be robust in practice and especially benefits from a good starting point, i.e., one close to the constraint boundary. The optimal charge-control current is computed by minimizing the PMTP objective function in (13), which consists of computing a control law that resembles a tracking problem subject to constraints as in (14) and listed in Table 1.

In order to compute an estimate of maximum available charge and discharge power, we need first to solve the PMTP for fast-charge and fast-discharge, respectively. We define $\underrightarrow{\boldsymbol{r}}_{k+1} = \overline{z} \cdot \boldsymbol{e}$ for charge and $\underrightarrow{\boldsymbol{r}}_{k+1} = \underline{z} \cdot \boldsymbol{e}$ for discharge in (13). Constraints are imposed on the terminal voltage, input current, SOC and cell core temperature; the constraint inequalities are defined as in [16].

For the self-adaptive solution, we compute the unconstrained optimal control input sequence by substituting for $\underrightarrow{\boldsymbol{z}}_{k+1}$ in (13) and solving the stationarity equation $dJ/d\underrightarrow{\Delta \boldsymbol{i}}_{k+1} = 0$ for $\underrightarrow{\Delta \boldsymbol{i}}_{k+1}$, (similar to (6)), to obtain

$$\underrightarrow{\Delta \boldsymbol{i}}^*_{k+1} = -\frac{1}{2} H_z^{-1} \boldsymbol{g}_z, \tag{15}$$

where

$$H_z = \left(G_z^\mathsf{T} G_z + \rho_k I_{N_\mathrm{c}} \right)^{-1} \boldsymbol{g}_z = -2 G_z^\mathsf{T} \left(\underrightarrow{\boldsymbol{r}}_{k+1} - \Phi \tilde{A} \boldsymbol{\chi}_k - N_z \right).$$

and matrix N_z accounts for affine terms in the CET model equations (introduced in Section 4); see [18] for additional details.

3.1 Time scales

The time scales used in the proposed SOP algorithm are the same as those used in our previous work [12] and are illustrated in Fig. 1. The basic idea is that at every time step k_i of a drive cycle of length N_{sim} we wish to compute the battery state of power over a duration of ΔT seconds. Therefore, we run the self-adaptive MPC every l-th step within the power prediction interval to compute the instantaneous power P_l. The SOP algorithm is designed with a prediction horizon N_p.

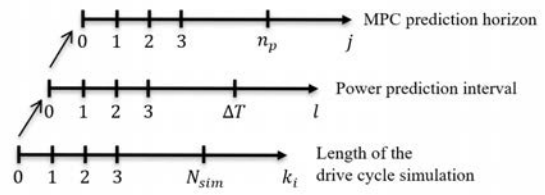

Figure 1: SOP algorithm time scales.

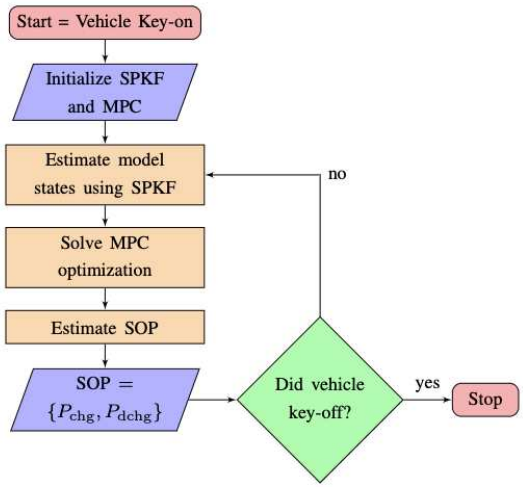

Figure 2: High-level SOP estimation algorithm flowchart.

3.2 SOP estimation algorithm

The SOP estimation algorithm comprises three main steps: (i) state estimation using a sigma-point Kalman filter (SPKF), (ii) solution to the MPC optimization problem, and (iii) SOP calculation. A high-level flow chart describing the algorithm is shown in Fig. 2. At each sampling point, the algorithm obtains values for the time-varying linear state-space matrices and then executes the MPC optimization to compute a value for instantaneous power P_l. The algorithm then numerically integrates all instantaneous power values over a specified power-prediction window of ΔT seconds in order to obtain the total energy able to be inserted (charge) or extracted (discharge) to/from the battery cell during the specified interval. This value is then averaged to produce a single estimate of the maximum sustainable power. The steps are summarized in Algorithm 1; since the initialization process is the same as in [12], we omit it here for brevity.

4 CET model and state estimation

To demonstrate the proposed method, we shall use the low-order coupled electro-thermal (CET) model whose battery charge-control architecture was first presented in [16] along with the details of the CET model development. Characterization results for a $2.5\ \mathrm{Ah}$ 26650 (model ANR26650m1-b) $\mathrm{LiFePO_4}$ (LFP) battery from A123 appear in the same work. The CET model captures terminal voltage, SOC, voltage hysteresis, and surface and core temperatures in a five-state model. The dynamics are described by the coupling of internal heat generation represented by a two-state thermal model with a three-state electrical equivalent-circuit model. It is important to note that the electrical equivalent-circuit model parameters are themselves temperature dependent and are updated at each time step with respect to the core temperature estimate using a look-up table computed offline. We refer the reader to [16] for a detailed discussion of the model, the associated state equations, and the linearization process needed for the MPC framework.

Accurate knowledge of internal battery states is vitally important in order to maximize battery performance, extend battery life and ensure operation within design limits. However, most internal battery states cannot be directly measured, e.g., SOC and core temperature. In this context, we rely on an optimal estimator to estimate these states in real time using available current, voltage and temperature measurements. In this work, we adopt a sigma-point Kalman filter (SPKF), a non-linear, derivative-free version of the Kalman filter (KF) algorithm [19]. The main idea of the SPKF algorithm is that at each time step, a set of points (sigma points) is chosen so that the possibly weighted mean and covariance of the points exactly matches the mean and covariance of the prediction of the present state (which is based on past data). A cloud of points is obtained by propagating this set of points through the nonlinear functions of the system. Then, the estimate of the true state at the present time step (which is based on

Algorithm 1 SOP estimation algorithm.

1. Power prediction loop

(a) For $l = 1, ..., \Delta T$:

i - Using the sub-sequences to compute Φ_k and G_k

If $l = 1$ **then** no sub-sequences exist. Linearize the model around $(\hat{x}^+_{k_i}, i_{k_i})$ and assume non-linear terms and model parameters constant throughout the prediction horizon when computing Φ_k, G_k and N_k .

else use the sub-sequences $\underrightarrow{\boldsymbol{i}}^{\text{tail}}_{k:k+n_p}$, $\boldsymbol{x}^{\text{tail}}_{k:k+n_p}$ and $\underrightarrow{\boldsymbol{v_{oc}}}^{\text{tail}}_{k:k+n_p}$ to compute Φ_k, G_k and N_k.

ii - Compute the adaptive input weight ρ.

iii - Solve the PMTP problem

$$\min_{\underrightarrow{\Delta \boldsymbol{i}}_{k+1}} J_k, \text{ s.t } M\underrightarrow{\Delta \boldsymbol{i}}_{k+1} \leq \boldsymbol{\gamma},$$

for "fast-charge" or "fast-discharge" over the prediction horizon N_p. The solution is the sequence of input increments $\underrightarrow{\triangle \boldsymbol{i}^*}_{k+1}$

iv - According to the receding horizon principle, compute the optimal input current as following

If $l = 1$ **then** $i_l = i_{k,i} + \triangle i^*_{k+1}$.

else $i_l = i_{l-1} + \triangle i^*_{k+1}$.

v - Compute states and output using i_l.

vi - Compute instantaneous power as $P_l = i_l \times v_l$,

vii - Using the prediction tail $\underrightarrow{\Delta \boldsymbol{u}}^{\text{tail}}_{k+1}$, compute the sub-sequence of future inputs $\underrightarrow{\boldsymbol{i}}^{\text{tail}}_{k:k+n_p}$, which is then used to compute the subsequences of states and OCV, $\boldsymbol{x}^{\text{tail}}_{k:k+n_p}$ and $\underrightarrow{\boldsymbol{v_{oc}}}^{\text{tail}}_{k:k+n_p}$, respectively. (b) Compute trapezoidal integral over the prediction window to obtain total energy, E_{tot,k_i}, (c) Compute available power estimate $P^{\text{chg}}_{\text{min},k_i}$, or $P^{\text{dis}}_{\text{max},k_i}$, as $E_{\text{tot},k_i} / (\Delta T \times T)$.

2. System update

(a) Get state estimates $(\hat{x}_{k_i})$ and uncertainty estimates (σ_x) from SPKF output and get i_{k_i} from measurement

3. Repeat Steps 1 and 2 until $k_i = N_{\text{sim}}$

all measurements taken up to and including the present time step) is obtained by approximating it to the mean and covariance of this cloud of points. Next we briefly describe the SPKF implementation for the CET model. The interested reader is directed to [20] for a full account on the SPKF algorithm and its use with the battery model.

In order to implement the SPKF algorithm we first assume that the CET model may be in discrete-time state-space model form as

$$\boldsymbol{x}_k = f(\boldsymbol{x}_{k-1}, \boldsymbol{u}_{k-1}, \boldsymbol{\omega}_{k-1}) \boldsymbol{y}_k = h(\boldsymbol{x}_k, \boldsymbol{u}_k, \boldsymbol{\nu}_k) \tag{16}$$

where $\boldsymbol{x}_k \in \mathbb{R}^{n_x}$ is the system state vector at time index k and is defined as

$$\boldsymbol{x}_k = \begin{bmatrix} z_k & i_{r,k} & h_k & T_{c,k} & T_{s,k} \end{bmatrix}^T$$

where $n_x = 5$ is the number of states. The function $f(\cdot)$ denotes a system of first order difference equations. The input to the system is $\boldsymbol{u}_k \in \mathbb{R}^2$, a vector containing the applied current i_k and the cooling temperature $T_{f,k}$. Vector $\boldsymbol{\omega}_k \in \mathbb{R}^2$, $\boldsymbol{\omega} \sim \mathcal{N}(0, \boldsymbol{\Sigma}_\omega)$ includes the stochastic process noise that models the respective current and cooling temperature sensor measurement errors that affect the system state. Thus,

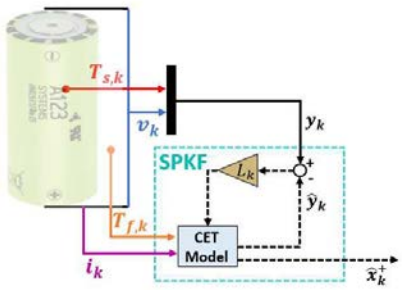

Figure 3: State estimation scheme.

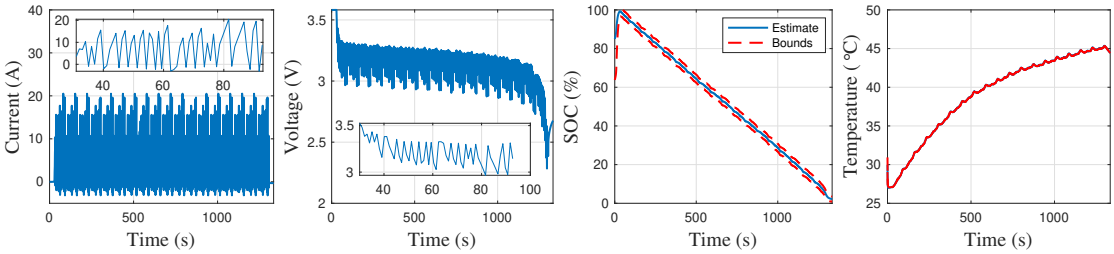

(a) Measured input current. (b) Measured voltage. (c) SPKF SOC estimate. (d) SPKF temperature estimate.

Figure 4: Measured data and SPKF estimates for the electric racing car discharge profile. (a) Input current profile (b) Output cell voltage (c) SOC estimate (d) Core temperature estimate.

in this construction, the true cell current is $i_k + \omega_{1,k}$ and the true cooling temperature is $T_{f,k} + \omega_{2,k}$. The estimate of the measurable outputs of the system is computed by the output function $h(\cdot)$ and denoted by $\boldsymbol{y}_k \in \mathbb{R}^2$ which comprises the output cell terminal voltage v_k and the surface temperature $T_{s,k}$. Vector $\boldsymbol{\nu}_k \in \mathbb{R}^2$, $\boldsymbol{\nu} \sim \mathcal{N}(0, \boldsymbol{\Sigma}_\nu)$ models "sensor noise" that affects the measurement of the system outputs but does not affect the system state. Voltage and cooling temperature sensor measurements are used to make step-wise corrections to the state estimates; $\boldsymbol{\Sigma}_\omega$ and $\boldsymbol{\Sigma}_\nu$ are the process noise and measurements noise covariance matrices, respectively. The state estimation scheme using the CET model for a cylindrical cell is diagrammed in Fig. 3.

5 Simulation results and discussion

Experimental data have been gathered from a 2.5 Ah A123 26650 (model ANR26650m1-b) battery cell in order to investigate the performance of the proposed SOP prediction algorithm. The cell test was conducted using an Arbin Instruments BT-2000 High Precision Battery Tester, and comprised a high discharge profile representing a Formula SAE electric racing car completing an endurance test. During the profile, the cell is discharged from 100% to 2% SOC while placed inside a Cincinnati Sub-Zero environmental chamber in order to regulate the temperature environment of the battery. The temperature inside the thermal chamber was set at 30 °C for two hours prior to the experiment in order to ensure that the surface temperature and core temperature were in equilibrium. The input current, cell voltage, SOC and core temperature estimates appear in Fig. 4. The current and voltage profile for one profile 'lap' are shown zoomed-in in Figs. 4a and 4b, respectively.
Employing the MPC framework and the dataset displayed in Fig. 4, the algorithm presented in Section 3.2 was implemented using Matlab[3]. The simulation was run with a sampling interval of $T = 1$ sec using a power prediction interval of $\Delta T = 10$ sec. Weight Q was set to I and hard constraints were imposed

[3]Matlab code containing the algorithm is available for download from a Github repository [21].

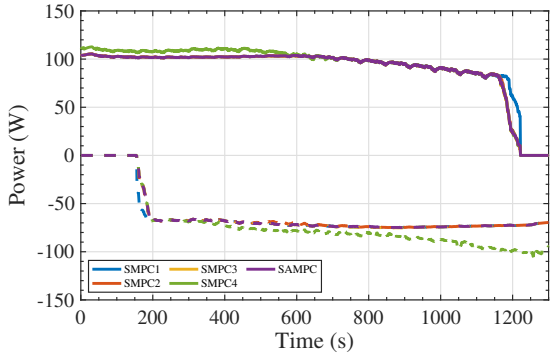

Figure 5: Charge and discharge SOP estimates for the electric racing car discharge profile.

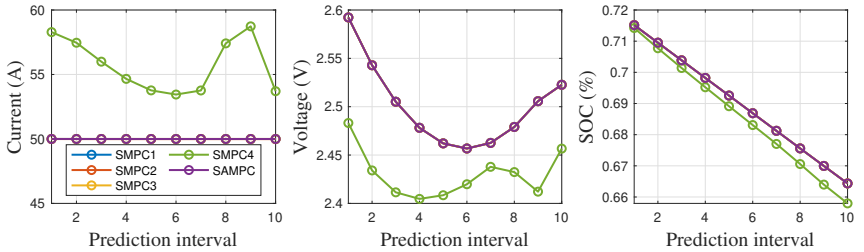

(a) Current. (b) Voltage. (c) SOC.

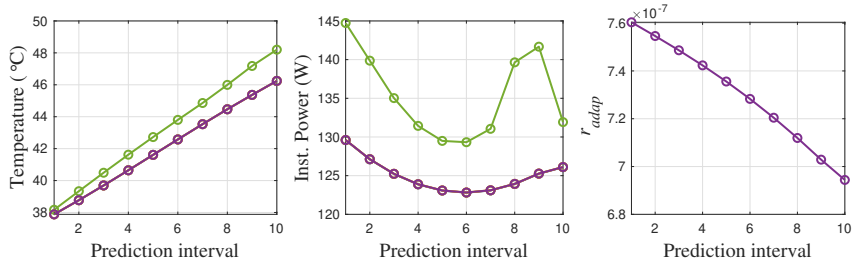

(d) Temperature. (e) Instantaneous power. (f) Adaptive input weighting for SAMPC.

Figure 6: Maximum discharge power limit prediction at k = 400 s.

on the applied current, set to remain between $-25\,\mathrm{A}$ and $0\,\mathrm{A}$ for charge, and $0\,\mathrm{A}$ and $50\,\mathrm{A}$ for discharge. Additionally, cell voltage was restricted to remain between $2.4\,\mathrm{V}$ and $3.6\,\mathrm{V}$ and the core temperature constrained to remain below $50\,^{\circ}\mathrm{C}$. A further MPC constraint was employed to keep SOC between $10\,\%$ and $95\,\%$. The charge and discharge SOP prediction simulation results appear in Fig. 5. In order to show the viability of achieving a more reliable SOP prediction policy using the proposed approach, we compare the simulation results against the standard MPC (SMPC) framework for SOP prediction presented in our previous work in [12] for four different input control weights: 10^{-6} (SMPC1), 10^{-7} (SPMC2), 10^{-8} (SPMC3) and 10^{-9} (SPMC4). The results for the SAMPC algorithm appear in purple in Fig. 5.

For this simulation, both SAMPC and SMPC algorithms were tuned with $N_{\mathrm{p}} = 3$ and $N_{\mathrm{c}} = 2$. It can be verified in Fig. 5 that SMPC1 and SMPC4 computed very distinct estimates at both high and low SOC stages. On the other hand, SMPC2 and SMPC3 computed very similar estimates to SAMPC, which indicates that the input weighting for tuning the MPC-based algorithm should lie within that range to give good results. In order to give some insight into the step-wise operation of the MPC algorithm, we present its output for the maximum discharge power calculation at time step $k_i = 400\,\mathrm{sec}$ of the test profile. MPC results are shown in Fig. 6 for (a) applied current, (b) terminal voltage, (c) SOC, (d) internal temperature, (e) the resulting calculation of instantaneous power over the 10-second N_{p} prediction interval and (f) adaptive input weighting for SAMPC.

It can be verified in Fig. 6, the QP algorithm computes an infeasible solution for SMPC4, where the state and output constraints are kept within its limits but the input current constraint is violated. In contrast, all the other algorithms computed maximum discharging current at its limit and kept the battery states within its bounds. The adaptive input weighting of SAMPC is shown in Fig. 6f and one can verify that its values changed throughout the prediction interval within the same order as SMPC2.

At low SOC, SMPC1 computed more discharge power available than all the other algorithms, as shown in Fig. 5. Taking a closer look inside of the prediction interval in Fig. 7, one can verify that SMPC1 computes an infeasible solution and the SOC state constraint is violated while the other constraints are kept within its limits. Note that in this time step, SAMPC computed the adaptive input weighting of the same order as SMPC3 as shown in Fig. 8.

Finally, we analyze the discrepancy between SMPC4 and the other algorithms for the charge SOP estimates in Fig. 5. Figure 8 shows the maximum charge power calculation at time step $k_i = 1200\,\mathrm{sec}$. Once again, SMPC4 computes an SOP estimate that violates the input current constraint. On the other hand, all the other algorithms computed the same maximum charge power profile. As shown in Fig. 8f, the SAMPC algorithm computed the adaptive input weighting as the same order as SMPC2.

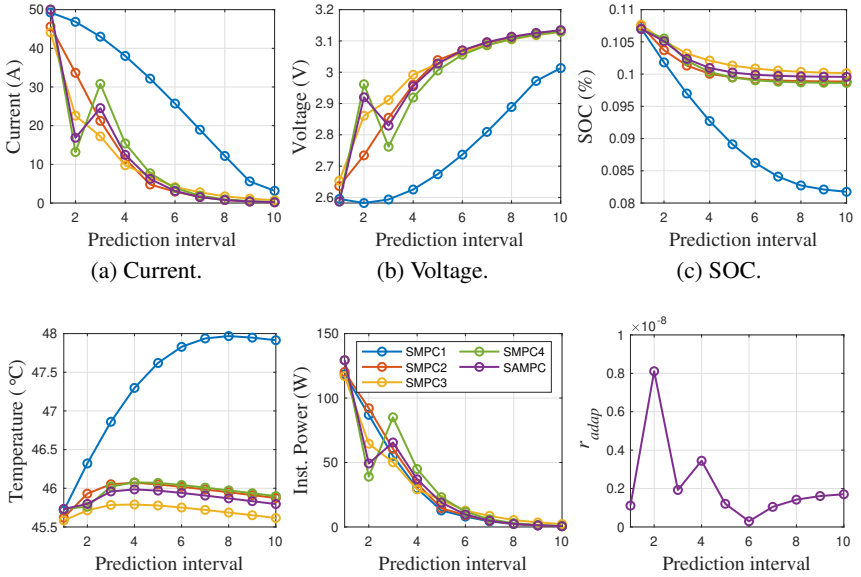

(a) Current. (b) Voltage. (c) SOC.

(d) Temperature. (e) Instantaneous power. (f) Adaptive input weighting for SAMPC.

Figure 7: Maximum discharge power limit prediction at k = 1200 s.

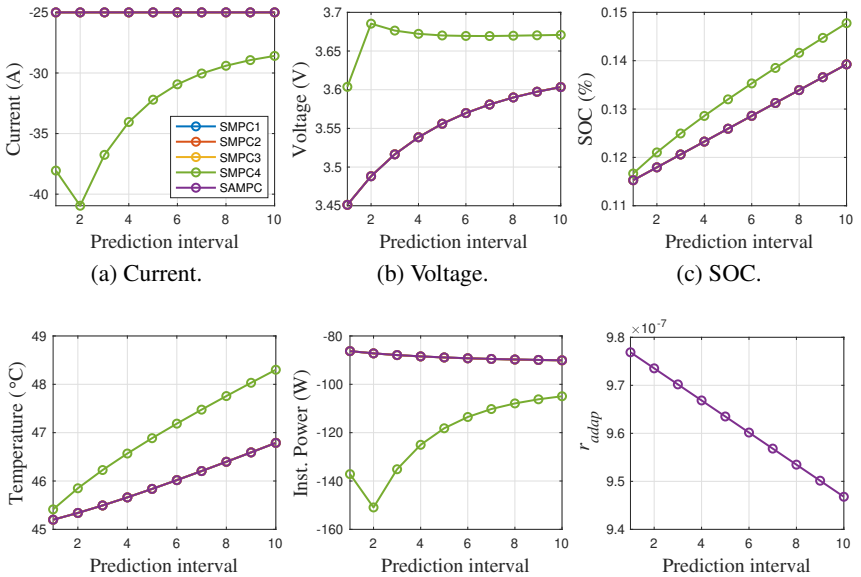

(a) Current. (b) Voltage. (c) SOC.

(d) Temperature. (e) Instantaneous power. (f) Adaptive input weighting for SAMPC.

Figure 8: Maximum charge power limit prediction at k = 1200 s.

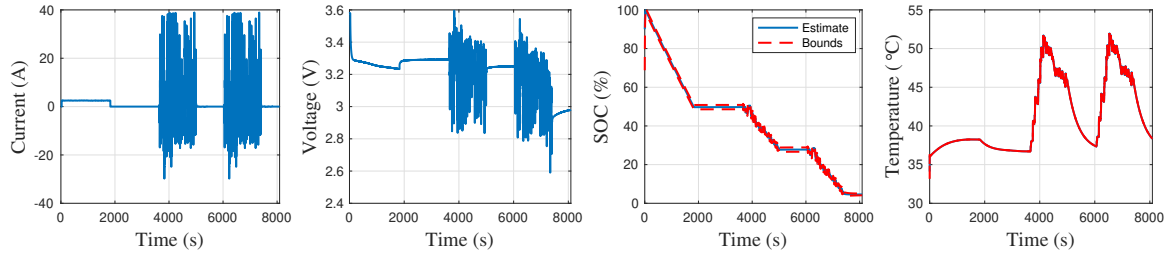

(a) Measured input current. (b) Measured voltage. (c) SPKF SOC estimate. (d) SPKF temperature estimate.

Figure 9: Measured data and SPKF estimates for the UDDS cycle profile. (a) Input current profile (b) Output cell voltage (c) SOC estimate (d) Core temperature estimate.

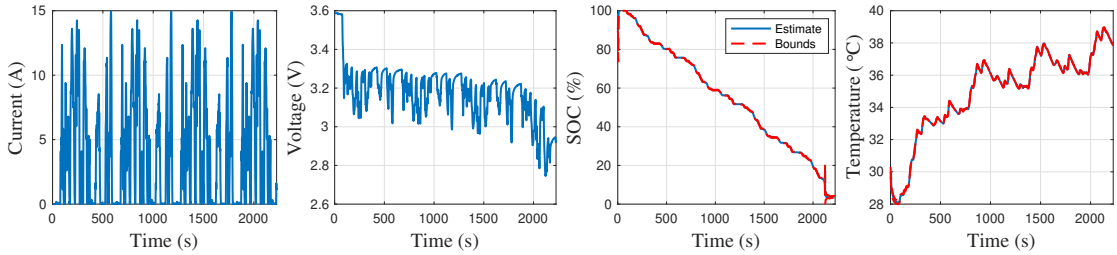

(a) Measured input current. (b) Measured voltage. (c) SPKF SOC estimate. (d) SPKF temperature estimate.

Figure 10: Measured data and SPKF estimates for the NYCC cycle profile. (a) Input current profile (b) Output cell voltage (c) SOC estimate (d) Core temperature estimate.

In order to investigate the robustness of the proposed MPC-based SOP estimation framework, simulations were run for two other drive cycles (using the same simulation setup): UDDS and NYCC. The measured data and SPKF estimates for the UDDS cycle profiles appear in Fig. 9 and comprise a constant discharge current profile followed by two UDDS cycles. The measured data and SPKF estimates for the NYCC cycle profiles appear in Fig. 10 and show four NYCC cycles. The SOP estimates for the UDDS and NYCC cycle profiles appear in Figs. 11 and 12, respectively. One can verify that the SOP estimates for both drive cycles were very consistent compared to the first test set presented at the start of this section, which indicates that the proposed MPC-based SOP estimation algorithm informed by the SPKF algorithm can be implemented for different applications.

6 Summary

This paper presents an MPC-based SOP estimation algorithm that uses an adaptive input weighting scheme that improves overall accuracy and robustness for the algorithm. Previous implementations revealed variations in computed SOP values; the proposed method selects starting points for the quadratic program optimization closer to the constrained targets, resulting in more reliable convergence to correct constrained solutions. The proposed method is computationally simple and relies on simple norms obtained for certain matrices involved in the problem solution.

References

[1] A. Arce, A. J. del Real, and C. Bordons, "MPC for battery/fuel cell hybrid vehicles including fuel cell dynamics and battery performance improvement," *J. Process Control*, vol. 19, no. 8, pp. 1289–1304, Sep. 2009.

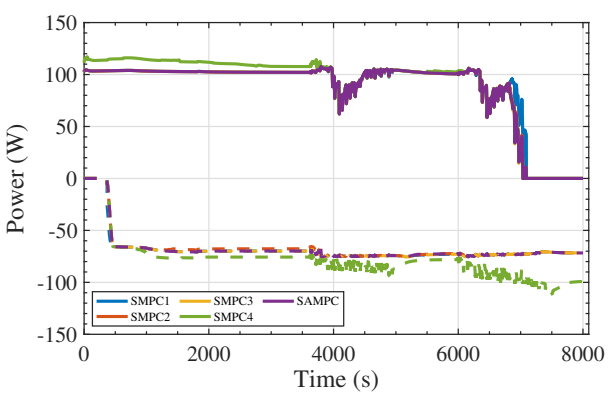

Figure 11: Charge and discharge SOP estimates for the UDDS discharge profile.

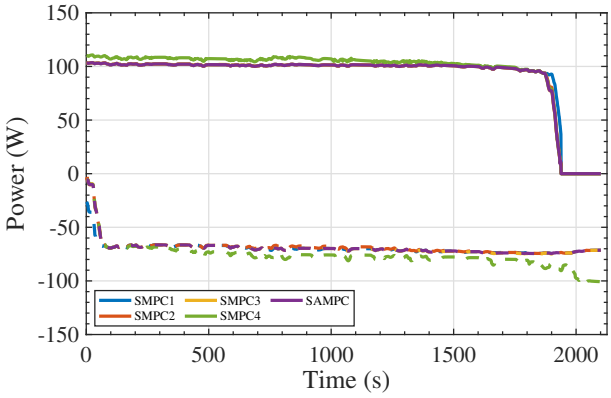

Figure 12: Charge and discharge SOP estimates for the NYCC discharge profile.

[2] A. Boehm and J. Weber, "Adaptives verfahren zur bestimmung der maximal abgebaren oder aufnehmbaren leistung einer batterie," DE Patent WO 2011/095368 A1, Aug. 11, 2011.

[3] G. L. Plett, "High-performance battery-pack power estimation using a dynamic cell model," *IEEE Trans. Veh. Technol.*, vol. 53, no. 5, pp. 1586–1593, Sep. 2004.

[4] R. D. Anderson, Y. Zhao, X. Wang, X. G. Yang, and Y. Li, "Real time battery power capability estimation," in *2012 American Control Conference (ACC)*, Jun. 2012, pp. 592–597.

[5] X. Hu, R. Xiong, and B. Egardt, "Model-based dynamic power assessment of lithium-ion batteries considering different operating conditions," *IEEE Trans. Industr. Inform.*, vol. 10, no. 3, pp. 1948–1959, Aug. 2014.

[6] T. Wik, B. Fridholm, and H. Kuusisto, "Implementation and robustness of an analytically based battery state of power," *Journal of Power Sources*, vol. 287, pp. 448 – 457, 2015.

[7] G. Dong, J. Wei, and Z. Chen, "Kalman filter for onboard state of charge estimation and peak power capability analysis of lithium-ion batteries," *J. Power Sources*, vol. 328, pp. 615 – 626, 2016.

[8] C. Burgos-Mellado, M. E. Orchard, M. Kazerani, R. Cárdenas, and D. Sáez, "Particle-filtering-based estimation of maximum available power state in lithium-ion batteries," *Applied Energy*, vol. 161, pp. 349 – 363, 2016.

[9] S. Mohan, Y. Kim, and A. G. Stefanopoulou, "Estimating the power capability of li-ion batteries using informationally partitioned estimators," *IEEE Transactions on Control Systems Technology*, vol. 24, no. 5, pp. 1643–1654, 2016.

[10] C. Zou, A. Klintberg, Z. Wei, B. Fridholm, T. Wik, and B. Egardt, "Power capability prediction for lithium-ion batteries using economic nonlinear model predictive control," *J. Power Sources*, vol. 396, pp. 580–589, 2018.

[11] M. Esfandyari *et al.*, "A hybrid model predictive and fuzzy logic based control method for state of power estimation of series-connected lithium-ion batteries in hevs," *J. Energy Storage*, vol. 24, p. 100758, 2019.

[12] M. A. Xavier, A. K. de Souza, G. L. Plett, and M. Scott Trimboli, "A low-cost mpc-based algorithm for battery power limit estimation," in *2020 American Control Conference (ACC)*, 2020, pp. 1161–1166.

[13] C. Hildreth, "A quadratic programming procedure," *Naval research logistics quarterly*, vol. 4, no. 1, pp. 79–85, 1957.

[14] M. A. Xavier and M. S. Trimboli, "Lithium-ion battery cell-level control using constrained model predictive control and equivalent circuit models," *J. Power Sources*, vol. 285, pp. 374–384, 2015.

[15] ——, "Lithium-ion battery cell-level control using constrained model predictive control and equivalent circuit models," *J. Power Sources*, vol. 285, pp. 374–384, 2015.

[16] A. K. de Souza, "Advanced predictive control strategies for lithium-ion battery management using a coupled electro-thermal model," Master's thesis, University of Colorado at Colorado Springs, 2020.

[17] A. V. Fiacco and G. P. McCormick, "The sequential unconstrained minimization technique for nonlinear programing, a primal-dual method," *Management Science*, vol. 10, no. 2, pp. 360–366, 1964.

[18] M. A. Xavier, A. K. de Souza, and M. S. Trimboli, "An lpv-mpc inspired battery sop estimation algorithm using a coupled electro-thermal model," in *2021 American Control Conference (ACC)*. IEEE, 2021, pp. 4421–4426.

[19] R. Van Der Merwe *et al.*, "Sigma-point kalman filters for probabilistic inference in dynamic state-space models," Ph.D. dissertation, OGI School of Science & Engineering at OHSU, 2004.

[20] G. L. Plett, "Sigma-point Kalman filtering for battery management systems of LiPB-based HEV battery packs: Part 1: Introduction and state estimation," *J. Power Sources*, vol. 161, no. 2, pp. 1356–1368, Oct. 2006.

[21] A. K. de Souza, "https://github.com/aloisiohks/LFP26650-SOPalgorithmMPC."

Authors

Aloisio Kawakita de Souza received his M.S. degree in Electrical Engineering with an option in Battery Controls from the University of Colorado Colorado Springs where he is currently a Ph.D. candidate in Electrical Engineering. He is also a Graduate Research Assistant with the Department of Electrical and Computer Engineering where he conducts both theoretical and experimental sponsored research on advanced modeling and control methods. His research interests include modeling, system identification, state estimation, and advanced control methods applied to lithium-ion batteries for automotive applications.

Dr. Plett received his Ph.D. in Electrical Engineering from Stanford University and is now Professor of Electrical and Computer Engineering at the University of Colorado Colorado Springs. His research focuses on topics in control systems as applied to the management of high-capacity battery systems, such as found in electric vehicles. Current research efforts include: physics-based reduced-order modeling of ideal lithium-ion dynamics and degradation mechanisms; nondestructive parameter estimation for physics-based models; estimation of cell electrochemical and degradation state; state-of-charge and state-of-health estimation; life-extending power-prediction methods.

Dr. Trimboli received his Ph.D. in Control Engineering from Oxford University and is now Associate Professor of Electrical and Computer Engineering at the University of Colorado Colorado Springs. His research focuses on topics in control systems as applied to the management of high-performance battery systems. Current research efforts include: physics-based reduced-order modeling of ideal lithium-ion dynamics; MPC for battery fast-charge and power limit estimation for life extension; battery state estimation using Kalman filters; life-extending power-prediction methods.